Dissolution Kinetics of Calcium Ions in Hydrothermal Demineralization of Eucalyptus

Yan Li,[a,b] Baojuan Deng,[a,b] Yajun Hou,[a,b] Shanshan Wang,[a,b] Fanyan Zeng,[a,b] Yadan Luo,[a,b] Jiayan Ge,[a,b] and Shuangquan Yao [a,b,*]

Alkali and alkali earth metals (AAEM) can be removed from lignocellulosic biomass *via* a new demineralization process constituting hydrothermal treatment. The dissolution mechanism of AAEM in different demineralization processes has not been extensively studied. This study employed calcium as a representative of the AAEM group, and changes in the concentration of calcium ions during the hydrothermal demineralization of eucalyptus wood were studied. The dissolution kinetics were modelled using Fick's second law. The effects of the reaction temperature, hydrolysate pH, and holding time on the dissolution rate of calcium ions were investigated. The kinetic equation for calcium ion dissolution was expressed as $\ln(1.9532e^{0.0077T}/1.9532e^{0.0077T}-C) = (0.4257P^{-0.2142}e^{-10622.1/8.314T})t + \ln(1.9532e^{0.0077T}/1.056\times10^{-8}T^{3.5263}p^{0.4449})$. The activation energy of the reaction was 10.62 kJ/mol. The linear regression coefficient (R^2) of the predicted and experimental values was 0.9879, which implied high precision of the kinetic model. The results showed that the calcium ions underwent rapid internal diffusion and dissolution during hydrothermal demineralization. The study provides theoretical support for the efficient removal of alkali earth metals via hydrothermal demineralization.

DOI: 10.15376/biores.17.2.2849-2863

Keywords: Eucalyptus wood; Demineralization; Hydrothermal treatment; Alkali and alkali earth metals; Dissolution kinetics

Contact information: a: School of Light Industrial and Food Engineering, Guangxi University, Nanning, 530004, PR China; b: Guangxi Key Laboratory of Clean Pulp & Papermaking and Pollution Control, Nanning, 530004, PR China;
**Corresponding author: yaoshuangquan@sina.cn*

INTRODUCTION

Various issues including environmental pollution, greenhouse gasses, and resource shortages caused by the use of fossil-fuel-generated energy have gained much attention in recent years (Brennan and Owende 2010). Biomass energy is environmentally friendly, renewable, abundant, and it produces zero carbon emissions. The development and utilization of biomass energy is an effective strategy to mitigate these effects (Huber *et al.* 2006; Guo *et al.* 2015; Nabgan *et al.* 2017; Rodionova *et al.* 2017). Lignocellulosic biomass is the most abundant biomass resource on earth (Taha *et al.* 2016; Shrestha *et al.* 2017), and it can be used for the preparation of polymer materials, fine chemicals, and biological energy sources (Gallezot 2012). Research shows that the pyrolysis of lignocellulosic biomass to produce bio-oil is one of the best alternatives to traditional fossil energy (Alonso *et al.* 2010; Menon and Rao 2012; Taha *et al.* 2016). The yield and properties of bio-oil are affected by the type of feedstock, the pyrolysis temperature, and

alkali and the alkali earth metals (AAEM) content (Hassan *et al.* 2009; Mourant *et al.* 2011). The content of AAEM in biomass is low, but it has a significant effect on the production of bio-oil (Fahmi *et al.* 2008; Oudenhoven *et al.* 2016). In particular, the yield of bio-oil decreases, while the non-condensable gas and biochar yields increase (Wang *et al.* 2015) with increasing AAEM.

The effect of AAEM on the pyrolysis reaction is suppressed by removing a part of AAEM before pyrolysis through a process known as demineralization. It includes washing and pickling (Pittman *et al.* 2012; Das and Sarmah 2015; Wang *et al.* 2015; Kan *et al.* 2016). Mourant *et al*. (2011) used deionized water and dilute nitric acid to remove AAEM. The effects of AAEM on the preparation of bio-oil were investigated. A small increase in the sugar yield was observed by the removal of water-soluble AAEM (Rollag *et al.* 2020). Acid-soluble AAEM, particularly calcium and magnesium, are bound to the biomass in the form of calcium carboxylates. These are replaced by hydrogen during pickling. The compact structure of biomass is destroyed (Chaiwat *et al.* 2008). The production of sugar and other oligomers increases. Oudenhoven *et al.* (2015) found that the catalytic activity of AAEM was the main factor that affects the sugar yield. The catalytic activity of AAEM is passivated by acid, which promotes an increase in sugar production. However, the decomposition yield of lignin is reduced. Char agglomeration is promoted as the melting of lignin is inevitable (Rollag *et al.* 2020). In addition, the use of acid also leads to the degradation of a large amount of carbohydrate, and the production of biofuel decreases (Oudenhoven *et al.* 2015). Therefore, the traditional demineralization has many shortcomings, and it is important to develop green and efficient demineralization methods. The results show that AAEM was removed by the hydrothermal treatment. Dai *et al.* (2019) found that hydrothermal treatment significantly increased the content of aromatics by the effective removal of AAEM. The hydrothermal treatment catalyzed the conversion of levoglucosan (an important precursor of aromatics production) to hydroxyl compounds, which was inhibited, resulting in a significant increase in the aromatic yield. Ge *et al.* (2020) investigated the removal of potassium, calcium, and magnesium from eucalyptus wood by hydrothermal treatment. The pyrolysis products were found to be more concentrated, and the bio-oil yield was higher. Scott *et al.* (2001) studied the removal mechanism of potassium and calcium. The dissolution of potassium and calcium ions increased as the temperature increases. In addition, the pickling of wood dissolves more calcium ions than hydrothermal treatment. This can be attributed to the presence of calcium in the form of salt in biomass. The equilibrium of precipitation and dissolution of calcium salts is disturbed in an acidic environment. In addition, the tight bond between calcium ions and organic matter is broken. In general, there is little research on the mechanism of biomass demineralization.

Calcium ions, as metal ions commonly contained in plant cells, are characterized by their high content and complex forms (water-soluble and acid-soluble). Therefore, it is of great significance to study the dissolution of calcium ions in hydrothermal demineralization. In this study, changes in the concentration of calcium ions from eucalyptus wood during hydrothermal treatment were studied. The dissolution kinetics of calcium ions was modelled using Fick's second law. The effects of the reaction temperature, the hydrolysate pH, and the holding time on the dissolution rate of calcium ions were investigated. The equation for the dissolution kinetics of calcium ions during hydrothermal treatment was determined. The result provides theoretical insights into the efficient removal of alkali earth metals *via* hydrothermal treatment.

EXPERIMENTAL

Materials

The eucalyptus wood was obtained from local forest farms (Guangxi, China). The wood was cut into slices with lengths, thicknesses, and widths of 10 to 15 mm, 3 to 5 mm, and greater than 10 mm, respectively. The standard calcium solution was purchased from Agilent Technologies, Inc. (Palo Alto, CA, USA). Other analytical reagents were purchased from Shanghai Aladdin Bio-Chem Technology Co., Ltd. (Shanghai, China).

Methods

The hydrothermal treatment of eucalyptus chips was performed in six 1,000 mL stainless steel cylindrical reactors (Greenwood Products, Inc., Piscataway, NJ, USA). The ratio of solid to pure water was 1:6. The reaction temperature was 140 to 180 ℃. Hydronium ions are formed at high temperatures. In fact, the hydrolysis solution is acidic (pH <3) after hydrothermal pretreatment. The pH of the hydrolysate was adjusted using sodium hydroxide solution during hydrothermal pretreatment. The acidity in the hydrolysate is neutralized by the pre-addition of sodium hydroxide. Degradation of carbohydrates and lignin is inhibited by regulating pH during AAEMs removal. The final pH value was between 3 and 7. The holding time was 0 to 80 min. The solid and liquid were separated after the reaction. The hydrolysate was centrifuged at 10,000 rpm for 15 min. The supernatant was filtered and collected using a 0.45 μm membrane (Yao *et al.* 2017).

One milliliter of hydrolysate, 2 mL of hydrogen peroxide, and 5 mL of nitric acid were added to the digestion tank. The microwave digestion method has high digestion efficiency. *In situ* regeneration of nitric acid was induced by a series of reactions. The oxygen content in the gas phase of the digestion kettle is the key factor affecting the digestion reaction. The organic substrate is effectively oxidized by the addition of hydrogen peroxide.

The digestion tank was added into the microwave digestion device after the mixture complete mixing for 15 min to perform the digestion at 220 ℃ for 5 min. The hydrolysate was transparent and clear. The digested solution was transferred to a 25 mL volumetric flask and diluted three times using pure water. The diluted solution was filtered using a 0.22 μm membrane. The same method was used to prepare the blank samples (Pardinho *et al.* 2018).

The standard solution of calcium ions was progressively diluted using 5% dilute nitric acid solution. Standard solutions with different concentrations of 0, 0.5, 5, 10, and 20 mg/L were prepared and analyzed using an inductively coupled plasma spectrometer (ICP-OES; Optima 5300DV, Perkin Elmer, Waltham, MA, USA). The spectrometer was operated at a forward power of 1.2 kW, a plasma gas flow rate of 15 L/min, an auxiliary gas flow rate of 1.5 L/min, a nebulizing gas flow rate of 0.75 L/min, a solution uptake rate of 0.75 mL/min, and a waste drainage rate of 1.5 mL/min.

The instrument stability and solution uptake delay were 15 and 30 s, respectively. A wavelength of 422.7 nm was selected as the analytical line for the calcium ions, and a standard concentration curve was obtained (Pohl *et al.* 2018). The digested samples were analyzed.

RESULTS AND DISCUSSION

Kinetic Model

Calcium ions exist in different forms in eucalyptus cells, and are mainly present in ionic form or as a stable compound (Thyrel *et al.* 2021). Most of the stable form of calcium in plants exists in the form of calcium oxalate. Calcium oxalate is present in plants as crystals of different sizes and forms and can be deposited intracellularly and extracellularly. There are some calcium ions that combine with the carboxylate of organic matter (*e.g.* hemicellulose) to form stable forms of calcium. The dissolution of calcium ions is comprised of three steps. In the first step, the calcium ions in the eucalyptus cells dissolve during the solvent permeation into the eucalyptus wood. In step two, the calcium ions diffuse from the interior of eucalyptus to the solid-liquid interface. The solvent will react with calcium ions, and the intracellular calcium ions will be dissolved along the pores in the cell wall to the solid-liquid interface. Therefore, it is a typical internal diffusion behavior. In step three, the calcium ions diffuse from the solid-liquid interface to the solvent. Step two is the rate limiting step of the entire dissolution process, because the reaction rate and flow rate of solvent diffusion to the interior of the eucalyptus wood chips are at the same kinetic level as the reaction rate of the diffusion of calcium ions to the liquid-phase system. The outward diffusion of the solute is impeded by this reverse flow. The eucalyptus chips expand due to the solvent penetration, which prolongs the outward diffusion of the solute. In addition, many factors such as the density of the cell membrane and selective permeability can hinder solute dissolution. Therefore, the diffusion of calcium ions from the interior of eucalyptus wood to the solid-liquid interface is the rate-limiting step of dissolution, which is an unstable process.

The eucalyptus wood chip specimens had a flat shape. Calcium ions diffuse from the thick center of the eucalyptus wood to the solid-liquid interface. The diffusion points are symmetric on both sides of the eucalyptus chip. Therefore, the dissolution rate of calcium ions at any time is symmetrical on both sides of the chip. The mass transfer resistance of the cell wall is negligible. The solute diffusion of eucalyptus wood during hydrothermal treatment is one-dimensional diffusion. Therefore, the diffusion of calcium ions from the cell wall to the liquid-phase system is in an unstable diffusion state. This is consistent with Fick's second law of diffusion (Nicolin *et al.* 2016; Kozlova *et al.* 2019), which is described by Eq. 1.

$$\frac{\partial C}{\partial t} = \frac{D\partial^2 C}{\partial X^2} \quad (1)$$

where C is the dissolution rate of calcium ions in the reaction system at holding time t, D is the diffusion coefficient, and X is the distance (m)

It will be assumed here that the eucalyptus wood chip is a standard flat plate model (thickness is $2L$) and diffusion is considered only from one side. The dissolution kinetics of calcium ions conform to the series-type equation of Fick's law, as seen in Eq. 2,

$$\frac{C-C_\infty}{C_0-C_\infty} = \frac{4}{\pi}\sum_{n=0}^{\infty}\frac{(-1)^n}{2n+1} \times \cos\frac{(2n+1)\pi d}{2L} \times e^{-\frac{(2n+1)^2\pi^2 Dt}{4L^2}} \quad (2)$$

where C_∞ is the dissolution rate of calcium ions after an infinitely long time during hydrothermal treatment, and C_0 is the dissolution rate of calcium ions at a holding time of 0 min.

The main limiting step of calcium ion dissolution during hydrothermal treatment is internal diffusion. These immediately enter the liquid-phase system when calcium ions dissolve into the plant cell wall. Thus, Eq. 3 is obtained,

$$\frac{C-C_\infty}{C_0-C_\infty} = \frac{4}{\pi}\sum_{n=0}^{\infty}\frac{(-1)^n}{2n+1} \times e^{-\frac{(2n+1)^2\pi^2 Dt}{4L^2}} \quad (3)$$

The dissolution rate of the unsteady reaction process can be expressed as an infinite series. In general, the first term is sufficient, thereby making Eq. 4,

$$\frac{C-C_\infty}{C_0-C_\infty} = \frac{4}{\pi} \times e^{-\frac{\pi^2 Dt}{4L^2}} \quad (4)$$

Hemicellulose and AAEM are efficiently dissolved by adjusting the pH of the hydrolysate during hydrothermal treatment. Moreover, the degradation of cellulose and lignin is inhibited during dissolution (Yao *et al.* 2017). The dissolution yield of cellulose and lignin decreased to 1.93% and 5.09%. Therefore, the final pyrolysis reaction is promoted. Therefore, the optimal hydrothermal treatment is affected by the temperature and the pH value. The diffusion coefficient (*D*) is represented by Eq. 5,

$$D = D_y + D_s \quad (5)$$

where D_y is the diffusion coefficient of the traditional hydrothermal treatment, and D_s is the optimized diffusion coefficient for the hydrothermal treatment.

The internal components of plants are complex under actual reaction conditions. The effects of the temperature and the pH of the hydrolysate on AAEM dissolution are influenced. Therefore, the original diffusion coefficient is corrected. The diffusion coefficient (*D*) considering the interaction between the temperature and the hydrolysate pH is obtained using the Arrhenius equation (Waldemer *et al.* 2007; Chowdhury *et al.* 2011). Considering $\lambda = \pi^2 D/4L^2$ and taking the log of both sides of Eq. 4. The dissolution behavior of calcium ions during the optimized hydrothermal treatment can be expressed by Eq. 6,

$$\ln\frac{C_\infty}{C_\infty - C} = \lambda\, t + \ln\frac{\pi C_\infty}{4(C_\infty - C_0)} \quad (6)$$

The model expresses the relationship between the reaction temperature, the hydrolysate pH, the holding time, and the dissolution rate of calcium ions during hydrothermal treatment.

Effect of the Hydrolysate pH on the Dissolution of Calcium Ions

The effect of the hydrolysate pH (3, 4, 5, 6, and 7) on the dissolution of calcium ions was investigated at a fixed temperature (140 °C) during the hydrothermal treatment. The changes in the calcium ion dissolution with time in hydrolysate with different pH values were examined. The results are shown in Fig. 1.

Figure 1 shows that $\ln[C_\infty/(C_\infty - C)]$ increased as the reaction time increased at different pH values. In addition, the amplitude increased as the pH increased. This implies that the pH had a significant effect on the dissolution rate of calcium ions. The results showed a good linear correlation between $\ln[C_\infty/(C_\infty - C)]$ and the reaction time. Different linear fitting equations were obtained. The details are presented in Table 1. The variation range of the diffusion coefficient *D* was small at pH values between 5 and 7. This was due to the inhibition of hemicellulose dissolution in weakly acidic environments, which results in the inhibition of calcium ions dissolution as well. It was difficult for the stable calcium

compounds in the eucalyptus wood to dissociate into free calcium. The dissolution of free calcium in the liquid-phase decreases (Dauer and Perakis 2014). The dissolution of calcium ion was inhibited. The *D*-value increased significantly at pH 4. This was attributed to the use of water as the solvent for hydrothermal treatment. The acetyl and methoxy groups on the hemicellulose branched chain were detached without the addition of other acidic chemicals (Garrote *et al.* 2007; Vegas *et al.* 2008; Pu *et al.* 2013). The main degradation products were acetic acid and xylose. The acidity of the hydrolysate increased as the acetic acid concentration increased. Calcium was dissolved by an acid, which promoted the dissolution of calcium ions and significantly increased the *D*-value. It remained constant as the dissolution of the acid-soluble AAEM tended to be balanced under strongly acidic conditions at pH 3.

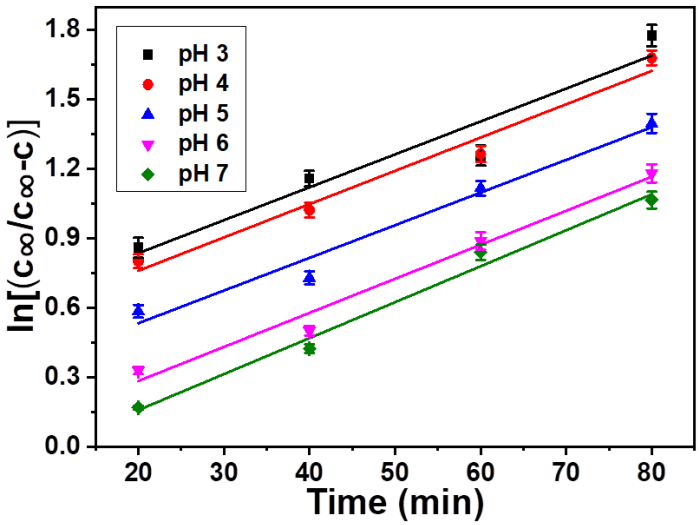

Fig. 1. Effect of the reaction time on ln[C_∞/(C_∞-C)] at different pH values of hydrolysates

Table 1. Relationship between ln[C_∞/(C_∞-C)] and the Reaction Time at Different pH Values of Hydrolysate

pH	Linear Fitting Equation	R^2
3	y=0.0151x+0.4980	0.9897
4	y=0.0150x+0.4381	0.9899
5	y=0.0134x+0.2919	0.9928
6	y=0.0130x+0.0902	0.9856
7	y=0.0129x+0.0061	0.9876

Effect of the Reaction Temperature on the Calcium Ion Dissolution

The effect of reaction temperature (140, 150, 160, 170, and 180 °C) on calcium ions dissolution was studied at a fixed hydrolysate pH (3). The changes in the calcium ion dissolution over time at different hydrolysis temperatures were investigated. The results are shown in Fig. 2.

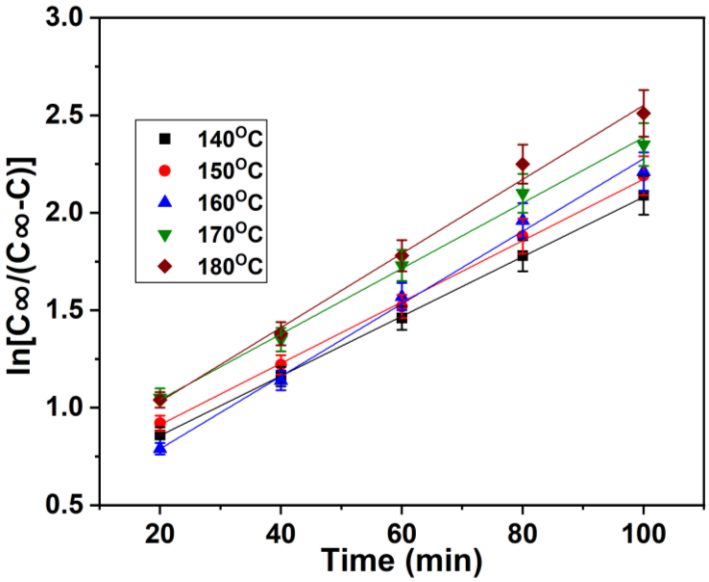

Fig. 2. Effect of the reaction time on ln[C_∞/(C_∞-C)] under different hydrolysis temperatures

Table 2. The Relationship between ln[C_∞/(C_∞-C)] and the Reaction Time Under Different Reaction Temperatures of Hydrolysates

Reaction Temperature (°C)	Linear Fitting Equation	R^2
140	y=0.0151x+0.4980	0.9837
150	y=0.0158x+0.5381	0.9903
160	y=0.0169x+0.5269	0.9878
170	y=0.0181x+0.5858	0.9892
180	y=0.0201x+0.5725	0.9909

Figure 2 shows that ln[C_∞/(C_∞-C)] increased with reaction time at different reaction temperatures. In addition, the amplitude increased as the temperature increased. This indicates that the reaction temperature had a significant effect on the dissolution of calcium ions. A linear correlation between ln[C_∞/(C_∞-C)] and the reaction time was observed. The different linear regression equations were obtained, as can be seen in Table 2. The variation in the D-value was less at low hydrothermal temperatures (140 to 150 °C). This was attributed to the fact that plant cells are not significantly damaged at low hydrothermal temperatures. The dissolution rate of calcium ions was low. The molecular thermal motion and carbohydrate degradation were inhibited at low temperatures due to the high resistance of calcium ions at the solid-liquid interface. However, the diffusion coefficient increased significantly as the reaction temperature increased when the hydrothermal treatment temperature was higher than 150 °C. This was due to the hydronium ions that were formed. Carbohydrate degradation was promoted due to acid autocatalysis. More formic acid and acetic acid were formed. This causes the concentration of acid in the liquid body to increase (Sun *et al.* 2020). The movement of acid-soluble calcium ions from the cell into the liquid-phase system was promoted, resulting in a significant increase in the dissolution rate of calcium ions. The steam pressure in the digestion tank increases at high temperatures, and the rapid dissolution of calcium ions from the inside of the cell was achieved.

Relationship between (C_∞-C_0), the Reaction Temperature, and the Hydrolysate pH during Hydrothermal Treatment

The above studies show that there was a good linear correlation between the hydrolysate pH, the reaction temperature, and the dissolution rate of calcium ions. However, the equilibrium dissolution rate of calcium ions varied with the reaction conditions. First, the effect of reaction temperature on the dissolution equilibrium rate C_∞ of calcium ions was studied. It was 140, 150, 160, 170, and 180 ℃, respectively. The results are shown in Fig. 3.

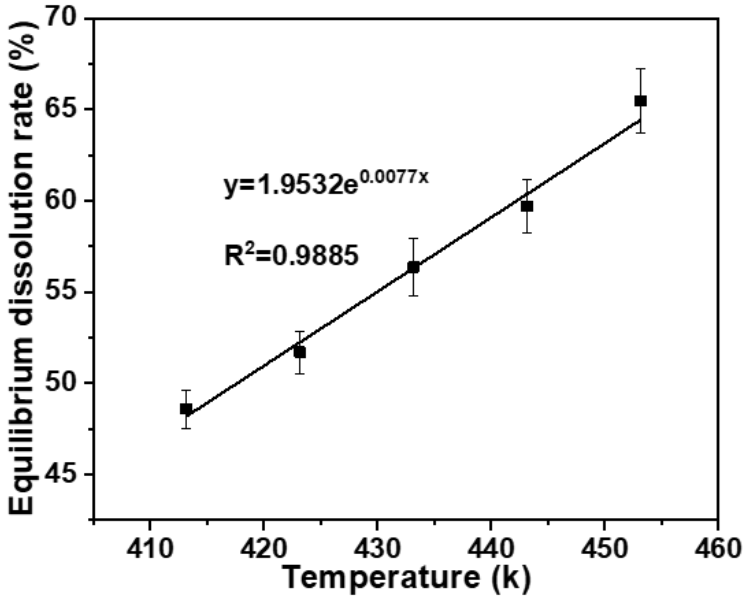

Fig. 3. Effect of the reaction temperature on the equilibrium dissolution rate of calcium ions

Figure 3 shows that the equilibrium dissolution rates (C_∞) of calcium ions at 140, 150, 160, 170, and 180 ℃ were 48.78, 51.70, 55.37, 58.68, and 67.46%, respectively. This indicates that the total amount of dissolved calcium ions increased as the reaction temperature increased. The exponential relationship between C_∞ and T was determined. The fitting curve is shown in Fig. 3. The equation $y = 1.95e^{0.0077T}$ was used to describe the equilibrium rate of calcium ion dissolution (C_∞) and the reaction temperature during the hydrothermal treatment of eucalyptus wood. The R^2-value of this equation was 0.9885, which indicated that the proposed reaction was real and effective.

C_0 varies with temperature and pH. The dissolution rate of calcium ions increases as with pH decreases. However, it increases as the reaction temperature increases. Combined with the above results, (C_∞-C_0), the reaction temperature, and the hydrolysate pH were related according to the exponential relationship shown in Eq. 7 and 8,

$$C_\infty - C_0 = \alpha T^\beta P^\gamma \quad (7)$$

$$\ln(C_\infty - C_0) = \ln \alpha + \beta \ln T + \gamma \ln P \quad (8)$$

where α, β, and γ are undetermined coefficients and P is pH. The relationship between ln(C_∞-C_0), ln$T$, and ln$P$ was obtained. The results are shown in Fig. 4 and 5.

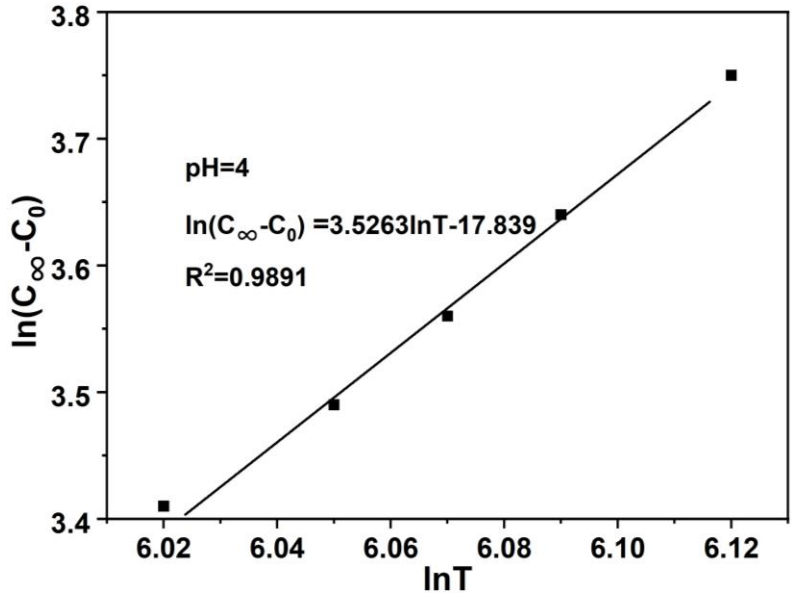

Fig. 4. Relationship between ln(C_∞-C_0) and ln$T$

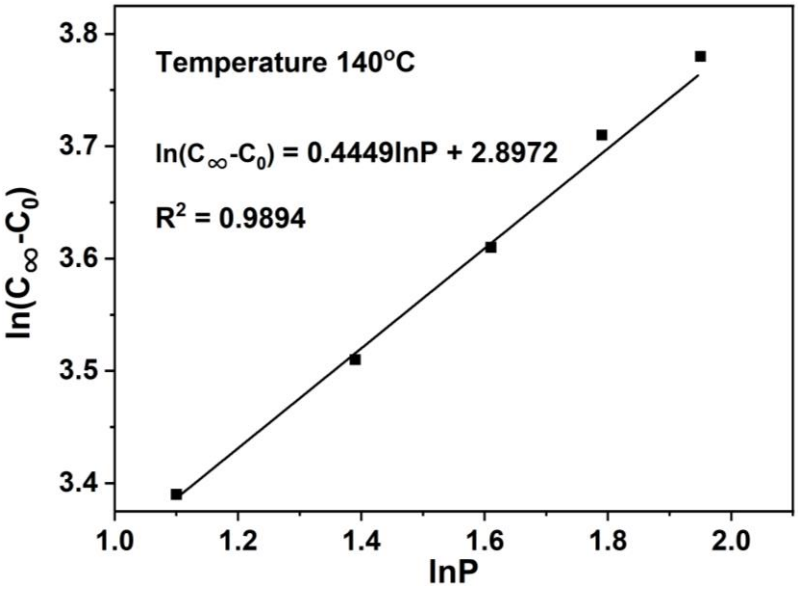

Fig. 5. Relationship between ln(C_∞-C_0) and ln$P$

The data in Fig. 4 and 5 are fitted according to Eq. 9 and 10, respectively.

$$\ln(C_\infty - C_0) = 3.5263 \ln T - 17.839 \qquad R^2=0.9891 \qquad (9)$$

$$\ln(C_\infty - C_0) = 0.4449 \ln P + 2.8972 \qquad R^2=0.9894 \qquad (10)$$

The α, β, and γ values of 1.0560×10^{-8}, 3.5263, and 0.4449, respectively, were calculated using Eq. 9 and 10. The R^2-values of Eq. 9 and 10 were 0.9891 and 0.9894, respectively. Thus, the relationship between (C_∞-C_0), the reaction temperature, and the hydrolysate pH is represented by Eq. 11,

$$C_\infty - C_0 = 1.0560 \times 10^{-8} T^{3.5263} P^{0.4449} \qquad (11)$$

Effect of the Relationship Between the Reaction Temperature and the Hydrolysate pH on the Reaction Rate Constant

The dissolution of calcium ions at different reaction temperatures and pH values was studied. The reaction temperature was 140 to 180 °C, and the pH was between 3 and 7. The effect of the relationship between these two parameters on calcium ions dissolution was determined using the Arrhenius equation. The result is shown in Eq. 12,

$$K = ke^{-\frac{Ea}{RT}} = aPne^{-\frac{Ea}{RT}} \quad (12)$$

where K is the apparent rate constant, k is the pre-exponential factor, Ea is the activation energy (kJ/mol), a and n are the empirical parameters, and P is the hydrolysate pH.

Table 3. The Relative Parameters Obtained from the Curve of the Relationship between ln(C_∞-C_0) and the Holding Time (T)

No.	Temperature (°C)	pH	K	β	R^2
1	140	3	0.0151	0.4980	0.9837
2		4	0.0150	0.4381	0.9869
3		5	0.0134	0.2919	0.9828
4		6	0.0130	0.0902	0.9816
5		7	0.0129	0.0061	0.9706
6	150	3	0.0158	0.5381	0.9603
7		4	0.0156	0.4799	0.9721
8		5	0.0151	0.4361	0.9937
9		6	0.0144	0.3544	0.9897
10		7	0.0134	0.2130	0.9648
11	160	3	0.0169	0.5269	0.9878
12		4	0.0167	0.4533	0.9775
13		5	0.0157	0.2446	0.9709
14		6	0.0154	0.1108	0.9920
15		7	0.0151	0.0489	0.9853
16	170	3	0.0181	0.5858	0.9692
17		4	0.0186	0.3800	0.9937
18		5	0.0171	0.1593	0.9779
19		6	0.0166	0.0368	0.9847
20		7	0.0157	-0.0049	0.9855
21	180	3	0.0201	0.5725	0.9809
22		4	0.0193	0.3585	0.9790
23		5	0.0178	0.1315	0.9805
24		6	0.0170	0.0250	0.9804
25		7	0.0165	-0.0349	0.9741

As shown in Table 3, the apparent rate constant increased as the reaction temperature increased, and it and decreased as the pH increased. The apparent rate constant and the activation energy at different pH values were calculated in Table 4. The R^2 of all the fitting curves were greater than 0.90, which implied that the results were real and valid. The reaction activation energy was 10.62 kJ/mol, and it changed slightly under different reaction conditions. The relationship between the pre-exponential factor and the pH was expressed by Eq. 13 according to the above results.

$$k = aP^n \quad (13)$$

Table 4. The Apparent Rate Constants and the Activation Energies at Different pH Values

pH	ln(*k*)	E_a (kJ/mol)	R^2
3	- 1.0181	10.9720	0.9802
4	- 1.1397	10.5663	0.9896
5	- 1.1460	10.8115	0.9722
6	- 1.2331	10.6178	0.9891
7	- 1.4032	10.1431	0.9856

The empirical parameters, a and n, were calculated as ln(a)= −0.8541 and n= −0.2142. The relationship between the apparent rate constant, the reaction temperature, and the pH value was represented by the Arrhenius equation. Therefore, the apparent rate constant can be expressed by Eq. 14 and 15,

$$\ln k_1 = -0.8541 - 0.2142 \ln P - \frac{10622.1}{8.314T} \quad (14)$$

$$k_1 = 0.4257P^{-0.2142} \times e^{-\frac{10622.1}{8.314T}} \quad (15)$$

The dissolution kinetics model of calcium ions can be expressed by Eq. 16,

$$\ln \frac{1.9532e^{0.0077T}}{1.9532e^{0.0077T}-C} = \left(0.4257P^{-0.2142}e^{-\frac{10622.1}{8.314T}}\right)t + \ln \frac{1.9532e^{0.0077T}}{1.056\times10^{-8}T^{3.5263}P^{0.4449}} \quad (16)$$

where C is the dissolution rate (%) of calcium ions at holding time t (min), T is the reaction temperature (K), and P is the hydrolysate pH.

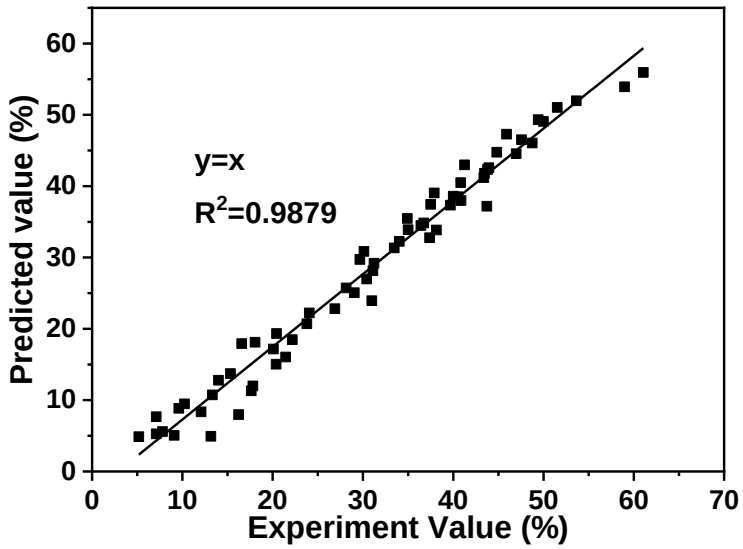

Fig. 6. The relationship between the experimental and predicted values in the calcium ion dissolution kinetics model

The kinetic model describes the relationship between the reaction temperature, the hydrolysate pH, the holding time, and the dissolution rate of calcium ions, which allows the prediction of alcium ions dissolution during hydrothermal demineralization. The accuracy of the model was analyzed. Figure 6 shows the relationship between the predicted and experimental values of calcium ion dissolution during hydrothermal demineralization. The R^2-value was 0.9879, which implied the high precision of the kinetic model.

CONCLUSIONS

1. A kinetic model for calcium dissolution during hydrothermal demineralization of eucalyptus wood was established using Fick's second law. The reaction temperature and hydrolysate pH during hydrothermal demineralization have significant effects on the dissolution of calcium ions.
2. A kinetic equation for the dissolution of calcium ions was established based on the change in the calcium ion dissolution rate under different reaction conditions. This equation affords a low reaction activation energy and high accuracy. The diffusion of calcium ions from the interior of eucalyptus to the solid–liquid interface is the rate-limiting step of dissolution, which implies that calcium ion dissolution is a typical internal diffusion process during hydrothermal demineralization.
3. The results of this work provide theoretical insights for the effective removal of AAEM from lignocellulosic biomass by hydrothermal demineralization.

ACKNOWLEDGMENTS

This project was sponsored by the National Natural Science Foundation of China (22078075). This project was supported by the Natural Science Foundation of Guangxi Province (2020GXNSFBA297164).

REFERENCES CITED

Alonso, D. M., Bond, J. Q., and Dumesic, J. A. (2010). "Catalytic conversion of biomass to biofuels," *Green Chemistry* 12(9), 1493-1513. DOI: 10.1039/C004654J

Brennan, L., and Owende, P. (2010). "Biofuels from microalgae—A review of technologies for production, processing, and extractions of biofuels and co-products," *Renewable and Sustainable Energy Reviews* 14(2), 557-577. DOI: 10.1016/j.rser.2009.10.009

Chaiwat, W., Hasegawa, I., Kori, J., and Mae, K. (2008). "Examination of degree of cross-linking for cellulose precursors pretreated with acid/hot water at low temperature," *Industrial & Engineering Chemistry Research* 47(16), 5948-5956. DOI: 10.1021/ie800080u

Chowdhury, S., Mishra, R., Saha, P., and Kushwaha, P. (2011). "Adsorption thermodynamics, kinetics and isosteric heat of adsorption of malachite green onto chemically modified rice husk," *Desalination* 265(1-3), 159-168. DOI: 10.1016/j.desal.2010.07.047

Dai, L., Wang, Y., Liu, Y., Ruan, R., He, C., Duan, D., Zhao, Y., Yu, Z., Jiang, L., and Wu, Q. (2019). "Bridging the relationship between hydrothermal pretreatment and co-pyrolysis: Effect of hydrothermal pretreatment on aromatic production," *Energy Conversion and Management* 180, 36-43. DOI: 10.1016/j.enconman.2018.10.079

Das, O., and Sarmah, A. K. (2015). "Mechanism of waste biomass pyrolysis: Effect of physical and chemical pre-treatments," *Science of the Total Environment* 537, 323-334. DOI: 10.1016/j.scitotenv.2015.07.076

Dauer, J. M., and Perakis, S. S. (2014). "Calcium oxalate contribution to calcium cycling

in forests of contrasting nutrient status," *Forest Ecology Management* 334, 64-73. DOI: 10.1016/j.foreco.2014.08.029

Fahmi, R., Bridgwater, A. V., Donnison, I., Yates, N., and Jones, J. M. (2008). "The effect of lignin and inorganic species in biomass on pyrolysis oil yields, quality and stability," *Fuel* 87(7), 1230-1240. DOI: 10.1016/j.fuel.2007.07.026

Gallezot, P. (2012). "Conversion of biomass to selected chemical products," *Chemical Society Reviews* 41(4), 1538-1558. DOI: 10.1039/C1CS15147A

Garrote, G., Kabel, M. A., Schols, H. A., Falqué, E., Domínguez, H., and Parajó, J.C. (2007). "Effects of *Eucalyptus globulus* wood autohydrolysis conditions on the reaction products," *Journal of Agricultural and Food Chemistry* 55(22), 9006-9013. DOI: 10.1021/jf0719510

Ge, J., Wu, Y., Han, Y., Qin, C., Nie, S., Liu, S., Wang, S., and Yao, S. (2020). "Effect of hydrothermal pretreatment on the demineralization and thermal degradation behavior of eucalyptus," *Bioresource Technology* 307, 123246. DOI: 10.1016/j.biortech.2020.123246

Guo, M., Song, W., and Buhain, J. (2015). "Bioenergy and biofuels: History, status, and perspective," *Renewable and Sustainable Energy Reviews* 42, 712-725. DOI: 10.1016/j.rser.2014.10.013

Hassan, E.-B. M., Steele, P. H., and Ingram, L. (2009). "Characterization of fast pyrolysis bio-oils produced from pretreated pine wood," *Applied Biochemistry and Biotechnology* 154(1-3), 182-192. DOI: 10.1007/s12010-008-8445-3

Huber, G. W., Iborra, S., and Corma, A. (2006). "Synthesis of transportation fuels from biomass: Chemistry, catalysts, and engineering," *Chemical Reviews* 106(9), 4044-4098. DOI: 10.1021/cr068360d

Kan, T., Strezov, V., and Evans, T. J. (2016). "Lignocellulosic biomass pyrolysis: A review of product properties and effects of pyrolysis parameters," *Renewable and Sustainable Energy Reviews* 57, 1126-1140. DOI: 10.1016/j.rser.2015.12.185

Kozlova, S., Mialdun, A., Ryzhkov, I., Janzen, T., Vrabec, J., and Shevtsova, V. (2019). "Do ternary liquid mixtures exhibit negative main Fick diffusion coefficients?," *Physical Chemistry Chemical Physics* 21(4), 2140-2152. DOI: 10.1039/C8CP06795C

Menon, V., and Rao, M. (2012). "Trends in bioconversion of lignocellulose: Biofuels, platform chemicals & biorefinery concept," *Progress in Energy and Combustion* 38(4), 522-550. DOI: 10.1016/j.pecs.2012.02.002

Mourant, D., Wang, Z., He, M., Wang, X. S., Garcia-Perez, M., Ling, K., and Li, C.-Z. (2011). "Mallee wood fast pyrolysis: Effects of alkali and alkaline earth metallic species on the yield and composition of bio-oil," *Fuel* 90(9), 2915-2922. DOI: 10.1016/j.fuel.2011.04.033

Nabgan, W., Abdullah, T. A. T., Mat, R., Nabgan, B., Gambo, Y., Ibrahim, M., Ahmad, A., Jalil, A. A., Triwahyono, S., and Saeh, I. (2017). "Renewable hydrogen production from bio-oil derivative via catalytic steam reforming: An overview," *Renewable and Sustainable Energy Reviews* 79, 347-357. DOI: 10.1016/j.rser.2017.05.069

Nicolin, D. J., Rossoni, D. F., and Jorge, L. M. M. (2016). "Study of uncertainty in the fitting of diffusivity of Fick's second law of diffusion with the use of bootstrap method," *Journal of Food Engineering* 184, 63-68. DOI: 10.1016/j.jfoodeng.2016.03.024

Oudenhoven, S. R. G., van der Ham, A. G. J., van den Berg, H., Westerhof, R. J. M., and Kersten, S. R. A. (2016). "Using pyrolytic acid leaching as a pretreatment step in a

biomass fast pyrolysis plant: Process design and economic evaluation," *Biomass and Bioenergy* 95, 388-404. DOI: 10.1016/j.biombioe.2016.07.003

Oudenhoven, S. R. G., Westerhof, R. J. M., and Kersten, S. R. A. (2015). "Fast pyrolysis of organic acid leached wood, straw, hay and bagasse: Improved oil and sugar yields," *Journal of Analytical and Applied Pyrolysis* 116, 253-262. DOI: 10.1016/j.jaap.2015.09.003

Pardinho, R. B., Vecchia, P. D., Mendes, A. L. G., Bizzi, C. A., Mello, P. A., Duarte, F. A., and Flores, E. M. M. (2018). "Determination of toxic elements in yerba mate by ICP-MS after diluted acid digestion under O_2 pressure," *Food Chemistry* 263, 37-41. DOI: 10.1016/j.foodchem.2018.04.112

Pittman, C. U., Mohan, D., Eseyin, A., Li, Q., Ingram, L., Hassan, E.-B. M., Mitchell, B., Guo, H., and Steele, P. H. (2012). "Characterization of bio-oils produced from fast pyrolysis of corn stalks in an auger reactor," *Energy & Fuels* 26(6), 3816-3825. DOI: 10.1021/ef3003922

Pohl, P., Szymczycha-Madeja, A., and Welna, M. (2018). "Simple ICP-OES based method for determination of selected elements in brewed ground and soluble coffees prior to evaluation of their intake and chemical fractionation," *Food Chemistry* 263, 171-179. DOI: 10.1016/j.foodchem.2018.04.127

Pu, Y., Hu, F., Huang, F., Davison, B. H., and Ragauskas, A. J. (2013). "Assessing the molecular structure basis for biomass recalcitrance during dilute acid and hydrothermal pretreatments," *Biotechnology for Biofuels* 6, 15. DOI: 10.1186/1754-6834-6-15

Rodionova, M. V., Poudyal, R. S., Tiwari, I., Voloshin, R. A., Zharmukhamedov, S. K., Nam, H. G., Zayadan, B. K., Bruce, B. D., Hou, H. J. M., and Allakhverdiev, S. I. (2017). "Biofuel production: Challenges and opportunities," *International Journal of Hydrogen Energy* 42(12), 8450-8461. DOI: 10.1016/j.ijhydene.2016.11.125

Rollag, S. A., Lindstrom, J. K., and Brown, R. C. (2020). "Pretreatments for the continuous production of pyrolytic sugar from lignocellulosic biomass," *Chemical Engineering Journal* 385, 123889. DOI: 10.1016/j.cej.2019.123889

Scott, D. S., Paterson, L., Piskorz, J., and Radlein, D. (2001). "Pretreatment of poplar wood for fast pyrolysis: Rate of cation removal," *Journal of Analytical and Applied Pyrolysis* 57(2), 169-176. DOI: 10.1016/S0165-2370(00)00108-X

Shrestha, S., Fonoll, X., Khanal, S. K., and Raskin, L. (2017). "Biological strategies for enhanced hydrolysis of lignocellulosic biomass during anaerobic digestion: Current status and future perspectives," *Bioresource Technology* 245(A), 1245-1257. DOI: 10.1016/j.biortech.2017.08.089

Sun, D., Sun, S.-C., Wang, B., Sun, S.-F., Shi, Q., Zheng, L., Wang, S.-F., Liu, S.-J., Li, M.-F., Cao, X.-F., *et al.* (2020). "Effect of various pretreatments on improving cellulose enzymatic digestibility of tobacco stalk and the structural features of co-produced hemicelluloses," *Bioresource Technology* 297, 122471. DOI: 10.1016/j.biortech.2019.122471

Taha, M., Foda, M., Shahsavari, E., Aburto-Medina, A., Adetutu, E., and Ball, A. (2016). "Commercial feasibility of lignocellulose biodegradation: Possibilities and challenges," *Current Opinion in Biotechnology* 38, 190-197. DOI: 10.1016/j.copbio.2016.02.012

Thyrel, M., Backman, R., Boström, D., Skyllberg, U., and Lestander, T. A. (2021). "Phase transitions involving Ca - The most abundant ash forming element - In thermal treatment of lignocellulosic biomass," *Fuel* 285, 119054. DOI:

10.1016/j.fuel.2020.119054
Vegas, R., Kabel, M., Schols, H. A., Alonso, J. L., and Parajó, J. C. (2008). "Hydrothermal processing of rice husks: Effects of severity on product distribution," *Journal of Chemical Technology and Biotechnology* 83(7), 965-972. DOI: 10.1002/jctb.1896
Waldemer, R. H., Tratnyek, P. G., Johnson, R. L., and Nurmi, J. T. (2007). "Oxidation of chlorinated ethenes by heat-activated persulfate: Kinetics and products," *Environmental Science & Technology* 41(3), 1010-1015. DOI: 10.1021/es062237m
Wang, K., Zhang, J., Shanks, B. H., and Brown, R. C. (2015). "The deleterious effect of inorganic salts on hydrocarbon yields from catalytic pyrolysis of lignocellulosic biomass and its mitigation," *Applied Energy* 148, 115-120. DOI: 10.1016/j.apenergy.2015.03.034
Yao, S., Nie, S., Zhu, H., Wang, S., Song, X., and Qin, C. (2017). "Extraction of hemicellulose by hot water to reduce adsorbable organic halogen formation in chlorine dioxide bleaching of bagasse pulp," *Industrial Crops and Products* 96, 178-185. DOI: 10.1016/j.indcrop.2016.11.046

Article submitted: February 18, 2022; Peer review completed: March 20, 2022; Revised version received and accepted: March 25, 2022; Published: April 1, 2022.
DOI: 10.15376/biores.17.2.2849-2863